Supplement of The Cryosphere, 15, 1485–1500, 2021
https://doi.org/10.5194/tc-15-1485-2021-supplement

The Cryosphere
Open Access

Supplement of

Snow depth mapping with unpiloted aerial system lidar observations: a case study in Durham, New Hampshire, United States

Jennifer M. Jacobs et al.

Correspondence to: Jennifer M. Jacobs (Jennifer.jacobs@unh.edu)

Table S1. Technical specifications of the project UAS

UAS	
UAS type	quadcopter
Manufacturer/Model	UAV-America / Eagle X8
Diameter	130 cm
Height	70 cm
Number of rotors	4
Rotor diameter	27.5 in (~70cm)
Motor Manufacturer/Model	KDE Direct / 7208
RPM/Volt (KV rating)	110 KV
Aircraft empty weight	8 kg
Aircraft weight at take-off (with payload)	16 kg
Flight time at take-off weight	~7 minutes
Tolerable wind speed (with payload)	5 m/s
Flight controller	Pixhawk PX4
Flight Batteries	22,000 mAh 6 Cell Lipo (2X)
Sensor Payload	
Gimble	Gremsy H7
IMU/GPS	Applanix APX-15
Lidar	Velodyne VLP-16
Payload weight	3 kg

Snow depth mapping with unmanned aerial systems lidar observations: A case study in Durham, New Hampshire, United States

S2 Boresight Calibration

The deployment of a lidar system mounted on a UAV platform for snow depth monitoring requires flight patterns designed for calculating boresight alignment and post-processing to ensure that point clouds are properly aligned (Painter et al., 2016). Provided that GNSS data are accurate, the most common reason for misalignment of point clouds is boresight angle errors (Li et al., 2019). Boresighting is the process of calculating the differences between lidar sensor and IMU roll, pitch, and yaw angle measurements to correct those errors in point clouds. Traditionally, boresighting calibration is performed using antiparallel flight lines in addition to a perpendicular flight line (Keyetieu and Seube, 2019). Due to battery flight time limitations, it was not possible to complete the flight pattern that is commonly used for boresighting alignment. Because of this, the first two antiparallel flight lines were leveraged for boresighting calibration. Offsets between sensor and IMU are calculated by observing misalignments between lidar data collected from different flight lines, and iteratively adjusting roll, pitch, and yaw angles of the IMU data to produce sub-datasets into the same planes. To determine roll offset, broad (10 m) along-path cross-sections over flat terrain were assessed, and to determine pitch offset narrow (1 m) across-path cross-sections in sloped terrain where the point clouds overlapped were used (Figure S3). Though not shown here, unique features were leveraged within the data acquisition region, including barn roofs and deciduous tree branches, to assess the resulting boresight angles (Kumari et al., 2011; Li et al., 2005). For this particular study, boresight calibration was performed manually and iteratively. Methods often require extensive user input (Li et al., 2005), however boresight calibration is an increasingly automated process with wide variation in algorithms and approaches (e.g. Maas, 2000; Kumari et al., 2011; Zhang et al., 2019). In future work, automated boresight calibration methods to improve the accuracy of point cloud data sets will be explored.

Figure S2 shows two examples of ground return point clouds before and after calibration in this study's field region. Uncalibrated boresight angles between the INS and lidar sensor can result in poorly aligned point clouds (i and iii). Red and blue arrows in (A) and (B) show approximate flight direction during data acquisition superimposed on the LAS point cloud. Roll alignment errors present well in anti-parallel flight lines (flight lines flown parallel to each other but in the opposite direction) over flat terrain. The top panel in Figure S3 addresses roll misalignment with (a) showing the LAS point cloud and the two flight lines flown in opposite directions. The lidar returns within the box marked in red in (a) are shown in (a1) and (a2) at an oblique view angle. Figure (a1) shows how boresight errors of roll angles present, while (a2) shows proper boresight alignment for roll. Figure (b) shows the approximate location of returns and flight lines used for pitch boresight alignment error demonstration (b1) and its correction (b2). Pitch misalignment presents well in anti-parallel flight lines in areas with terrain relief while viewing across the flight track, as opposed to along the flight track as with roll alignment.

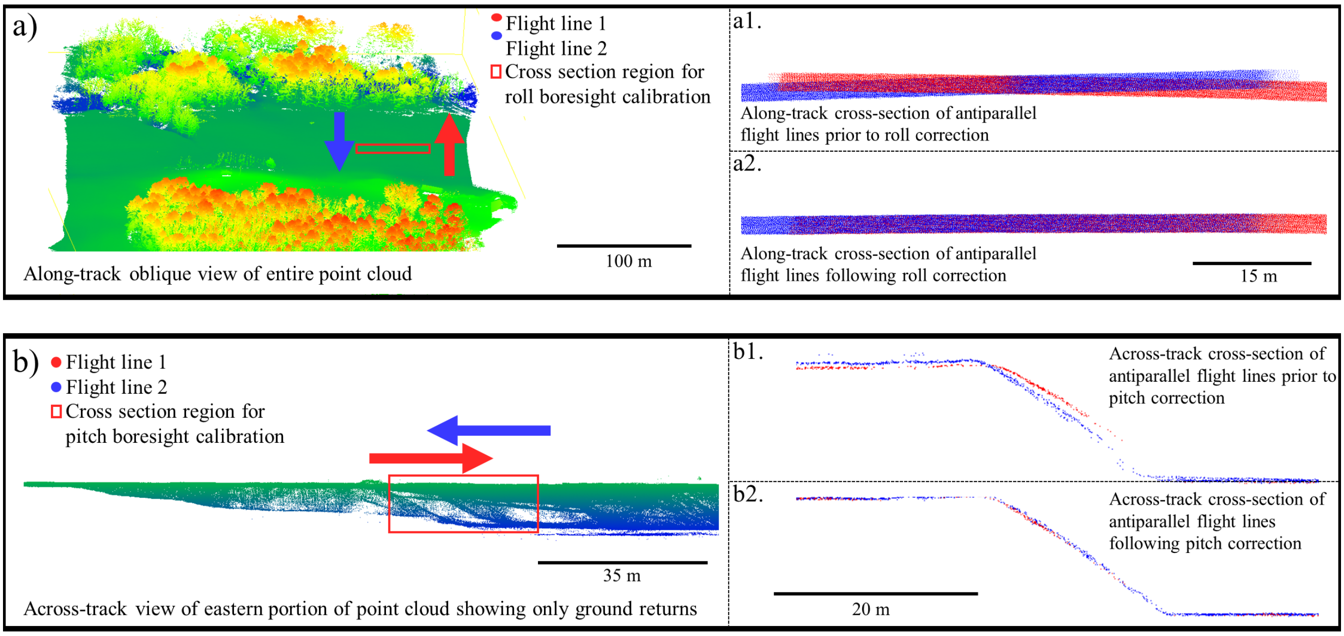

Figure S2. Boresight examples that show how uncalibrated boresight angles between the INS and lidar sensor can result in poorly aligned point clouds (a1 and b1). Arrows in (a) and (b) show approximate flight direction during data acquisition. The lidar returns within the box marked in red in (a) are shown in (a1) and (a2) at an oblique view angle. Figure (a1) shows how boresight errors of roll angles present, while (a2) shows proper boresight alignment for roll. Figure (b) shows the approximate location of returns used for pitch boresight alignment error demonstration (b1) and its correction (b2). Pitch misalignment presents well in anti-parallel flight lines in areas with terrain relief while viewing across the flight track, as opposed to along the flight track as with roll alignment. For (b, a1, a2, b1, and b2), only ground returns are shown for each flight line, while in (a), all returns are shown.

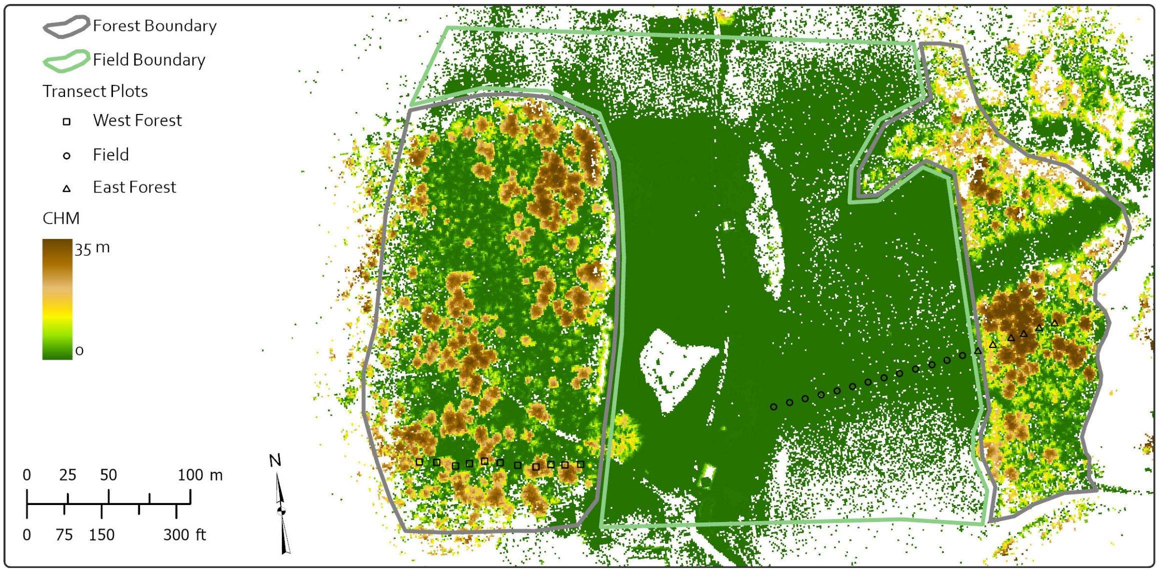

Figure S3. The Canopy Height Model (CHM) within the forest that was used to distinguish the intact upper canopy from other forest cover using our snow-off survey, collected with leaf off in the spring. The CHM was generated by subtracting the digital terrain model produced using ground-classified points from the digital surface model produced using all lidar points. This results in a digital model consisting solely of canopy heights with no terrain or topography. The CHM was determined from snow-off lidar point clouds on snow-off flight for 1 m^2 cells conducted on April 11, 2019.